

Cumulants and ordering of their ratios in 2D Potts models: Lessons for QCD?

Rajiv V. Gavai¹, Bedangadas Mohanty^{2,3}, Jaydev Singh Rao¹ and Swati Saha^{2,3}

¹*Department of Physics, Indian Institute of Science Education and Research Bhopal, Bhopal 462066, Madhya Pradesh, India**

²*School of Physical Sciences, National Institute of Science Education and Research, Jatni 752050, Odisha, India[†] and*

³*Homi Bhabha National Institute, Training School Complex, Anushaktinagar, Mumbai 400094, Maharashtra, India*

(Dated: December 20, 2023)

Theoretical considerations suggest an ordering of the ratios of net-baryon number fluctuations in the vicinity of the transition from the low-temperature hadronic phase to the high temperature quark-gluon plasma phase at small values of the baryon chemical potential, μ_B , in the QCD phase diagram. The ordering hierarchy is $\frac{\chi_6}{\chi_2} < \frac{\chi_5}{\chi_1} < \frac{\chi_4}{\chi_2} < \frac{\chi_3}{\chi_1}$, where χ_n is the n^{th} order cumulant of net-baryon number fluctuation. The STAR experiment observed this hierarchy in the ordering of cumulant ratios of net-proton number (a proxy of net-baryon number) for a range of colliding energies. These inequalities can be tested in spin models by taking the corresponding order parameters in the model as an analog of baryon density. We employed two different models: the two-state and three-state Potts models in two dimensions, which undergo a transition from an ordered phase to a disordered phase at their respective critical temperature. Simulations were performed on square lattices of different sizes using the Wolff algorithm. The cumulants of total magnetization are obtained up to the sixth order in both of these models in a temperature range near their corresponding critical temperatures. With increasing lattice size, height (trough) of the peaks (dips) of the higher-order cumulants appears to increase with the increase in the order of the cumulants. Except in a narrow range above the critical temperature of the three-state Potts model, the complete inequality or its complete reverse is not satisfied in the temperature ranges simulated.

I. INTRODUCTION

Understanding the phase structure and the nature of phase transitions in the temperature-baryon density (or equivalently the baryon chemical potential, μ_B) plane for the strongly interacting matter, known as quantum chromodynamics (QCD) phase diagram, is crucial for unraveling the fundamental properties of matter [1, 2]. While the QCD phase diagram is not well-explored for larger μ_B , the region below $\mu_B = 450$ MeV, spanning down to $\mu_B = 0$, has been extensively studied, both in theory [2, 3] and in experiments [4]. For vanishing and small values of μ_B , the transition from the low-temperature hadronic region to the quark-gluon plasma at high temperature is well-known to be a smooth transition (cross over) [5]. At larger values of μ_B , however, it is generally expected that a first-order phase transition line exists, which ends in a second-order critical point belonging to the three-dimensional Ising model universality class [6–8]. Comprehensive studies of net-proton fluctuations have been carried out with the Beam Energy Scan (BES) program of the Relativistic Heavy Ion collider (RHIC) in the STAR experiment to search for the QCD critical point [9, 10]. Recently, an ordering of the cumulant ratios of net-proton number, $\frac{\chi_6}{\chi_2} < \frac{\chi_5}{\chi_1} < \frac{\chi_4}{\chi_2} < \frac{\chi_3}{\chi_1}$, has been reported by the STAR experiment across the energy range 7.7 to 200 GeV [11] where χ_n is the n^{th} order cumulant of event-by-event net-proton number distribution. This ordering was suggested previously by

the Lattice-QCD (LQCD) calculations for the cumulants of net-baryon number fluctuations at small values of μ_B [12, 13]. Functional renormalization group (FRG) calculations were also found to follow this hierarchy of the inequalities [14]. In contrast, predictions from the Hadron Resonance Gas (HRG) model, utilizing an ideal gas equation of state within a grand canonical ensemble framework, consistently yield positive unity for all cumulant ratios, lacking the observed ordering [15]. One may wonder whether these inequalities are generically valid in the vicinity of any phase transition or even in wider regions surrounding it. In the QCD phase diagram, either near the cross over or near the QCD critical point, if it exists, whether such inequalities exist is an interesting question to ask.

With the advent of lattice gauge theories, the Z(N) spin models have gained significant importance in the study of critical behavior in SU(N) gauge theories at finite temperature. Here, the variable N in general represents the number of degrees of freedom: within SU(N) gauge theories, it denotes the number of colors comprising the gauge group, while in Z(N) spin models, it represents the number of distinct spin states assignable to each lattice site. Among the Z(N) spin models, the three-state Potts model (Z(3)) in three dimensions (3D) holds particular significance as it provides a valuable framework for understanding the phase structures of QCD based on the SU(3) gauge symmetry group. The Polyakov loop, which serves as an order parameter of SU(3) gauge theories, behaves similarly as spins in the low temperature phase of the 3D three-state Potts model [16, 17]. The line of first order phase transition in QCD phase diagram [18, 19] is closely related to the first order phase transition of 3D three-state Potts model in the absence of an exter-

* gavai@tifr.res.in

† bedanga@niser.ac.in

nal magnetic field [17, 20]. Addition of a small magnetic field (h) leads to a critical point in the Ising universality class for the three-state Potts model in 3D at h_c [21], making it a nice toy model to explore the hierarchy of inequalities of the ratios of net-baryon number cumulants. As a first step towards such an investigation, we studied the higher-order cumulants of magnetization in the two-state (Z(2)) and the three-state (Z(3)) Potts model on a two-dimensional lattice in this paper. Both are known to have critical points albeit of another universality class. The finite-size scaling of the higher-order cumulants of magnetization were investigated near the critical region in the respective models and the ordering of their ratios were tested.

The paper is structured as follows: in Sec. II, we provide an overview of the q -state Potts models, detailing their formalism and the computation of cumulants of magnetization up to 6th order in these models. We also discuss the application of finite size scaling relation, which enables the extraction of exponents associated with the scaling of higher-order cumulants. Section III presents the methodology employed for simulating the models and outlines the simulation validation process. In Sec. IV, we present the temperature-dependent behavior of cumulants and their ratios. The exponents involved with the finite-size scaling of the higher-order cumulants are estimated in terms of known critical exponents of the model and compared with the numerical results. Finally, Sec. V summarizes the key findings of our study.

II. MODEL AND OBSERVABLES

The Hamiltonian for the the q -state Potts model [22] is given by

$$\mathcal{H} = -\mathcal{J} \sum_{\langle i,j \rangle} \delta(\sigma_i, \sigma_j) - h \sum_i \delta(\sigma_i, 0), \quad (1)$$

where \mathcal{J} is a coupling constant in units of energy, determining the interaction strength among neighbouring spins, h is the external magnetic field applied to the model and δ is the Kronecker delta function. Here, σ_k can take any integer values in the set $\{0, 1, 2, \dots, (q-1)\}$ and for each σ_k , the spin orientations in the Potts model are represented by $s_k = \exp\left(\frac{i2\pi\sigma_k}{q}\right)$. The sum is over nearest neighbors $\langle i, j \rangle$. In d -dimensions there are $2d$ such pairs. We focus on $d = 2$ in this work. In the absence of an external magnetic field ($h = 0$), the model exhibits an exact symmetry represented by the group of permutations S_q , which encompasses all possible global permutations of the q spin values. This symmetry implies that each spin state is equally likely, and there is no preferred direction for alignment. However, below a critical temperature, the symmetry is spontaneously broken resulting in the alignment of spins along a specific direction and the establishment of an ordered phase. To measure the extent of symmetry breaking in the system, a quantity called

the order parameter is used, that provides a measure of the overall alignment of spins in the model. The order parameter for the q -state Potts model (m_{Potts}) that we use in this study is given by

$$m_{\text{Potts}} = \frac{q}{q-1} \left(\frac{\max(N_0, N_1, \dots, N_{q-1})}{N} - \frac{1}{q} \right), \quad (2)$$

where $N_\alpha = \sum_{j=1}^{L^d} \delta(\sigma_j, \alpha)$ with $\alpha \in \{0, 1, 2, \dots, q-1\}$ represents the number of sites in the lattice with $\sigma_i = \alpha$ and $N = L^d = \sum_\alpha N_\alpha$ is the total number of spin sites in the lattice.

In the following analysis and results, we will be dealing Potts model with both $q = 2$ and $q = 3$ states. The two-state Potts model is equivalent to the well-known Ising model for which the exact solution by Onsager gives the critical point at $T_C = \frac{2}{\ln(1+\sqrt{2})} \mathcal{J}/k_B \approx 2.2692 \mathcal{J}/k_B$ [23]. The three-state Potts model that belongs to the same universality class as the two-dimensional Ising model, undergoes a second order phase transition at $T_C = \frac{1}{\ln(1+\sqrt{3})} \mathcal{J}/k_B \approx 0.9950 \mathcal{J}/k_B$ [22].

A. Cumulants

In this paper, the main objects of interest are the higher-order cumulants (also referred as susceptibilities in the paper), which reflect the higher-order correlations amongst the spins. In spin models, the p^{th} order susceptibility normalized by the total number of spin sites in the lattice is defined [24] by

$$\chi_p(T) = \frac{1}{L^d \beta^p} \left(\frac{\partial^p \ln Z}{\partial h^p} \right)_{h \rightarrow 0}, \quad (3)$$

where $\beta = 1/(k_B T)$, T is the temperature, k_B is the Boltzmann constant. Here, Z is the partition function of the model given by its corresponding \mathcal{H} as

$$Z = \sum_a \exp(-\beta \mathcal{H}). \quad (4)$$

The sum over a in Eq. 4 means the summation over all possible spin configurations on the lattice. The higher-order spin-spin susceptibilities can be associated with the cumulants of total magnetization (M). This is because Z is proportional to the moment generating function [25] of M and therefore one can easily deduce,

$$\left(\frac{\partial^p \ln Z}{\partial h^p} \right)_{h \rightarrow 0} = \beta^p K_p(M). \quad (5)$$

Here, M is referred as magnetization which is equal to the product of the order parameter and the volume of the lattice, i.e., $M = L^d m_{\text{Potts}}$. $K_p(M)$ is the p^{th} order cumulant of M . The expressions for χ_p (obtained by using the relation of cumulants in terms of central moments

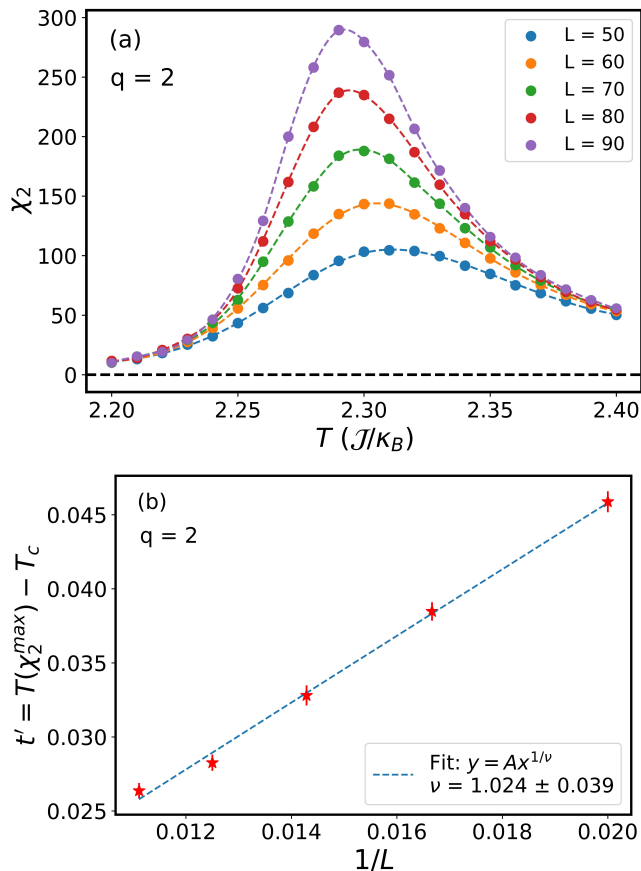


FIG. 1. (a) The second order susceptibility of magnetization for the two-dimensional Ising model (equivalent to $q = 2$ state Potts model) shown as a function of temperature. The results shown by different colored markers represent different lattice sizes (L). (b) The reduced temperature, $t' = T(\chi_2^{\max}) - T_c$ is plotted as a function of $1/L$, and fitted with the function $y = Ax^{1/\nu}$ to extract the value of ν .

[26]) up to $p = 6$ is listed below,

$$\chi_1 = \langle M \rangle / L^d \quad (6)$$

$$\chi_2 = \mu_2 / L^d \quad (7)$$

$$\chi_3 = \mu_3 / L^d \quad (8)$$

$$\chi_4 = (\mu_4 - 3\mu_2^2) / L^d \quad (9)$$

$$\chi_5 = (\mu_5 - 10\mu_3\mu_2) / L^d \quad (10)$$

$$\chi_6 = (\mu_6 - 15\mu_4\mu_2 - 10\mu_3^2 + 30\mu_2^3) / L^d \quad (11)$$

where $\mu_p = \langle (M - \langle M \rangle)^p \rangle$ is the p^{th} order central moment of the magnetization and the angular brackets, $\langle \dots \rangle$ represents average over all possible spin configurations on the lattice. We will be studying these χ_p 's as a function of temperature in the critical region.

B. Finite size scaling

In this section, we obtain the generalized relation for finite size scaling of the higher-order susceptibilities of magnetization in the Potts model. We define, $t = (T - T_c)/T_c$ and $h_r = \beta h$. For a second order (continuous) phase transition, there are at least two relevant scaling fields for the free energy: temperature like and magnetic field like. The dependence of free energy on these scaling fields near the critical point can be established by a bulk Renormalization Group (RG) transformation. RG transformation involves length scale re-scaling, under which, the scaling fields generally look like $C_1 L^{1/\nu} t$ and $C_2 L^{\Delta/\nu} h_r$, respectively [27, 28]. Here, the exponent ν is defined such that $\xi \sim t^{-\nu}$ (for a finite lattice $\xi \sim L$ at the critical point) and $\Delta \equiv \beta + \gamma$ is such that $\chi_1 \sim t^\beta$ and $\chi_2 \sim t^\gamma$ in the zero field limit, i.e., $h \rightarrow 0$.

In the obtained scaling relation for the singular part of the free energy after RG transformations, irrelevant scaling fields and non-linear contributions from relevant scaling fields can be safely removed by setting them to zero. This simplification is valid under the condition that $d < d_>$, where $d_>$ is the upper critical dimension. Consequently, only the linear order of temperature-like (t) and magnetic field-like (h_r) scaling fields remains, serving as the sole parameters that determine the distribution of the system [27]. The asymptotic finite size scaling relation of the singular part of *reduced free energy density*, i.e. $f_r^{(s)} = L^{-d} \ln Z$, can therefore be written as (for $t \rightarrow 0, h_r \rightarrow 0$)

$$f_r^{(s)}(t, h; L) \approx L^{-d} Y(C_1 L^{1/\nu} t, C_2 L^{\Delta/\nu} h_r). \quad (12)$$

Here, the function $Y(x, y)$ is same for every system in the universality class, i.e. it is universal, while the coefficients C_1 and C_2 are generally not universal. The n^{th} derivative of Eq. 12 with respect to h_r gives the scaling relation for the n^{th} order finite-size susceptibility,

$$\chi_n^{(s)}(t; L) \approx -C_2^n L^{\frac{n\Delta}{\nu} - d} \left. \frac{\partial^n Y}{\partial h_r^n} \right|_{h_r=0}. \quad (13)$$

From Eq. 13, we can extract the scaling relation for the singular part of χ_n , i.e., $\chi_n^{(s)} \sim L^{\frac{n\Delta}{\nu} - d}$. To simplify the exponents, we utilize the relations among the critical exponents: $\gamma = 2\Delta - (2 - \alpha)$ and $2 - \alpha = d\nu$. Both of these relations are valid for $d = 2$, but in general, the latter is only valid for any $d < d_>$. Thus, we can write the scaling exponent of n^{th} order susceptibility as,

$$e_n \equiv \frac{n\Delta}{\nu} - d = \frac{1}{2} \frac{n\gamma}{\nu} + (n - 2)d. \quad (14)$$

These exponents for $n = 2$ to 6 can now be calculated using the respective values of γ and ν for the model under consideration. For the $q = 2$ state Potts model on a two-dimensional lattice, we have $\gamma = \frac{7}{4}$ and $\nu = 1$ for $q = 2$ [29], while $\gamma = \frac{13}{9}$ and $\nu = \frac{5}{6}$ for $q = 3$ [22].

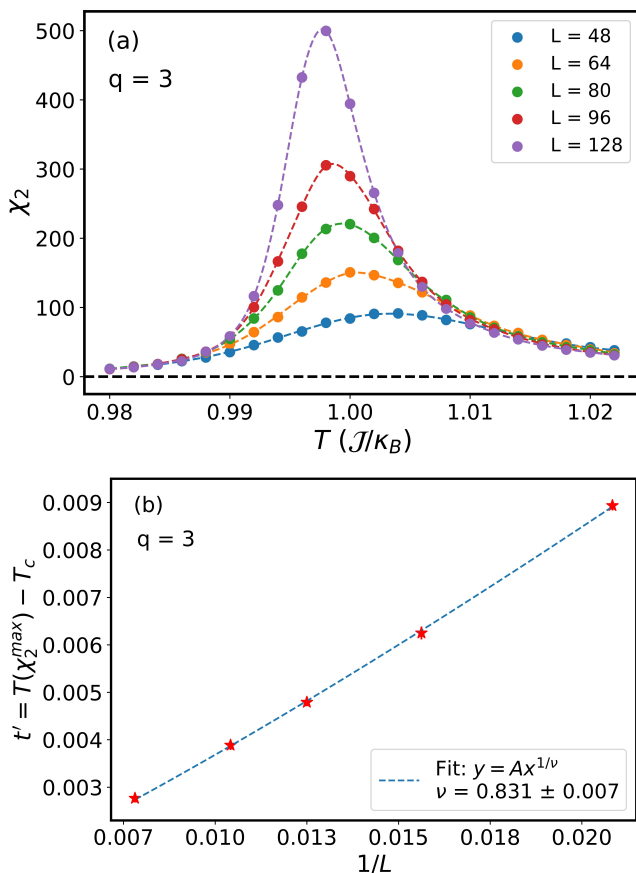


FIG. 2. (a) The second order susceptibility of magnetization for the two-dimensional $q = 3$ state Potts model shown as a function of temperature. The results shown by different colored markers represent different lattice sizes (L). (b) The reduced temperature, $t' = T(\chi_2^{\max}) - T_C$ is plotted as a function of $1/L$, and fitted with the function $y = Ax^{1/\nu}$ to extract the value of ν .

III. NUMERICAL SIMULATION

Both $q = 2$ and $q = 3$ state Potts model were simulated on two-dimensional lattices using the Wolff Cluster algorithm [30] at temperatures close to their corresponding critical temperature (T_C). In this algorithm, clusters of similarly oriented spin sites are determined randomly which are then flipped together to generate new states. This algorithm reduces the effect of critical slowing down near T_C with increase in lattice size, i.e. it has a smaller dynamical exponent resulting in more efficient simulations in this region [31]. For $q = 2$, square lattices of linear size $L = 50, 60, 70, 80$ and 90 were used in the simulations and during the simulation 10^4 independent configurations were generated after ensuring thermalization by throwing away sufficient initial configurations. Similarly, for $q = 3$, simulations were performed on square lattices with $L = 48, 64, 80, 96$ and 128 to generate 2×10^4 independent configurations after appropriate thermalization. In order to obtain independent spin configurations

on the lattice, configurations were recorded at the interval of 2τ where τ is the auto-correlation time that is obtained from the auto-correlation function (of M) defined in Eq. 15 using an exponential decay ansatz $\phi(t) \sim \exp(-\frac{t}{\tau})$.

$$\phi(t) = \frac{\langle M(0)M(t) \rangle - \langle M \rangle^2}{\langle M^2 \rangle - \langle M \rangle^2} \quad (15)$$

The magnetization is calculated for each spin configuration in the simulation and the higher-order susceptibilities of magnetization are calculated using Eqs. 6 - 11 by averaging over all possible spin configurations on the lattice.

IV. RESULTS

The top panels of Fig. 1 and Fig. 2 display the second-order susceptibility, denoted as χ_2 , for the $q = 2$ and $q = 3$ state Potts model respectively with varying lattice sizes, L . In both cases, χ_2 exhibits a distinctive peak structure. As may be expected, the locations ($T_{C,L}$) and magnitudes ($\chi_2(T_{C,L})$) of these peaks vary with changes in the lattice size. Their scaling behavior can be utilized to extract the critical exponents, specifically γ and ν , which will be further elaborated upon in the subsequent section, IV A.

A. Critical exponents

The critical exponents, γ and ν can be obtained using the scaling relations, $\chi_2(T_{C,L}) \propto L^{-\gamma/\nu}$ and $T_{C,L} - T_C \propto L^{-1/\nu}$, where $T_{C,L}$ is the pseudo-critical temperature for a given lattice size, and T_C represents the critical temperature of the model in the limit $L \rightarrow \infty$. The pseudo-critical temperature is an effective critical temperature observed in finite-sized systems, reflecting behavior similar to the critical point in infinite-sized systems. $T_{C,L}$ is defined as the location of the peak in the second order susceptibility, χ_2 distribution as shown in Figs. 1 and 2. By fitting χ_2 as a Gaussian function of the temperature, T , the peak location ($T_{C,L}, \chi_2(T_{C,L})$) is determined for each lattice size. The obtained values of $T_{C,L}$ and $\chi_2(T_{C,L})$ as a function of L are tabulated in Tables I and II for $q = 2$ and $q = 3$ state Potts model respectively. Also, we define the critical region around $T_{C,L}$ for each lattice size by the width of the χ_2 distribution peak, which is equal to the σ of the fitted Gaussian distribution function, represented here as σ_C . Using the values of $T_{C,L}$, the difference $t' = T_{C,L} - T_C$ is plotted as a function of $1/L$, and fitted with its scaling relations for both $q = 2$ and $q = 3$ state Potts model as shown in the bottom panels of Figs. 1 and 2 respectively. Alternatively, T_C can be estimated by plotting directly $T_{C,L}$ against L and fitting with $y = A + Bx^{-1/\nu}$. The resulting estimates ($T_C = 2.2780 \pm 0.0089$ for $q = 2$ and

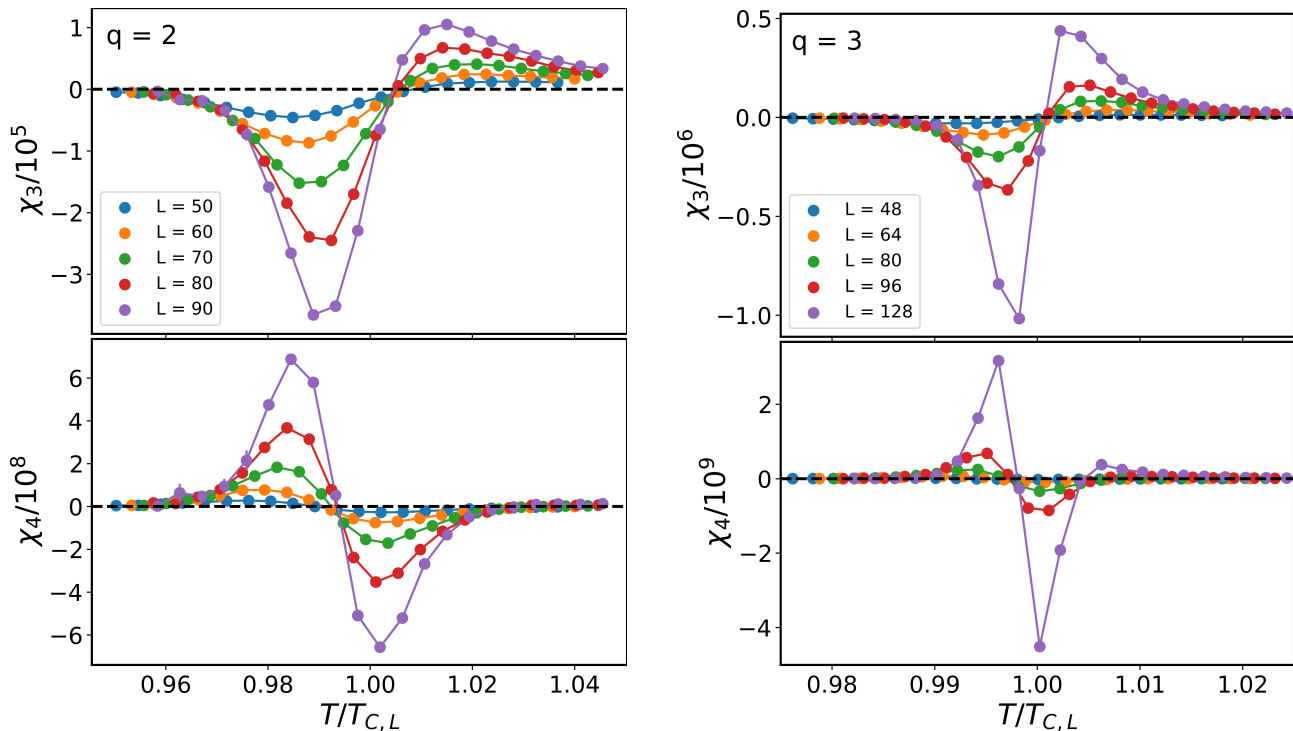


FIG. 3. The third and fourth order susceptibilities of magnetization, χ_3 and χ_4 , are shown for different lattice sizes as a function of temperature scaled by critical temperature of the corresponding lattice, $T/T_{C,L}$. The left side plot belongs to two-dimensional $q = 2$ state Potts model whereas the right side plot is for $q = 3$ state Potts model. The upper panel represents χ_3 and the bottom panel represents χ_4 [where χ_3 and χ_4 divided by a factor 10^5 (10^6) and 10^8 (10^9) respectively for $q = 2$ ($q = 3$)].

$T_C = 0.9953 \pm 0.0001$ for $q = 3$) are found to be consistent with the known values [22, 23] within uncertainties. For precise measurements of the critical exponents, however we employ the known values of T_C in the former method and extracted the coefficient ν . The peak position, $\chi_2(T_{C,L})$ as a function of L , is also fitted with its scaling relation. Therefore, the extracted values of γ and ν from the fits with the scaling relations are as follows: for $q = 2$, $\gamma = 1.758 \pm 0.060$, $\nu = 1.019 \pm 0.034$ whereas for $q = 3$, $\gamma = 1.435 \pm 0.014$, $\nu = 0.830 \pm 0.008$. The excellent agreement observed between the calculated values of γ and ν and their theoretical counterparts affirms the validation of our simulation.

Lattice size	$T_{C,L}$	$\chi_2(T_{C,L})$	σ_C
50	2.3151 ± 0.0007	105.656	0.0495 ± 0.0011
60	2.3076 ± 0.0006	143.913	0.0424 ± 0.0009
70	2.3020 ± 0.0007	188.497	0.0360 ± 0.0009
80	2.2974 ± 0.0005	238.766	0.0310 ± 0.0007
90	2.2956 ± 0.0005	289.739	0.0288 ± 0.0007

TABLE I. The extracted values for position ($T_{C,L}$), height ($\chi_2(T_{C,L})$) and width (σ_C) of the peak of χ_2 distribution as a function of temperature for $q = 2$ state Potts model. The quoted values after ' \pm ' represent statistical uncertainties derived from the fit.

We plot the higher-order susceptibilities, χ_3 and χ_4

Lattice size	$T_{C,L}$	$\chi_2(T_{C,L})$	σ_C
48	1.0039 ± 0.0001	105.656	0.0102 ± 0.0002
64	1.0012 ± 0.0001	143.913	0.0071 ± 0.0002
80	0.9998 ± 0.0001	188.497	0.0056 ± 0.0001
96	0.9989 ± 0.0001	238.766	0.0046 ± 0.0001
128	0.9978 ± 0.0001	289.739	0.0033 ± 0.0001

TABLE II. The extracted values for position ($T_{C,L}$), height ($\chi_2(T_{C,L})$) and width (σ_C) of the peak of χ_2 distribution as a function of temperature for $q = 3$ state Potts model. The quoted values after ' \pm ' represent statistical uncertainties derived from the fit.

for both $q = 2$ and $q = 3$ state Potts model in Fig. 3 as a function of temperature scaled by $T_{C,L}$. Since, these χ_n 's are one order derivative of its preceding χ_{n-1} (for $n > 2$), the sign of peak structure gets reversed in χ_n with respect to χ_{n-1} . Similarly, χ_5 and χ_6 are shown as a function of $T/T_{C,L}$ for both the models in Fig. 4. The height of the peaks or dips in these higher-order susceptibilities are found to be lattice size dependent. They also follow a scaling as a function of L as discussed in section II B. In order to determine the scaling exponents of the higher-order susceptibilities, we fit the maximum or minimum value of χ_n , depending on which is prominent, as a function of L against the scaling relation: $\chi_n^{\max/\min} \propto L^b$. The scaling exponents of χ_3 , χ_4 , χ_5 and χ_6 obtained from

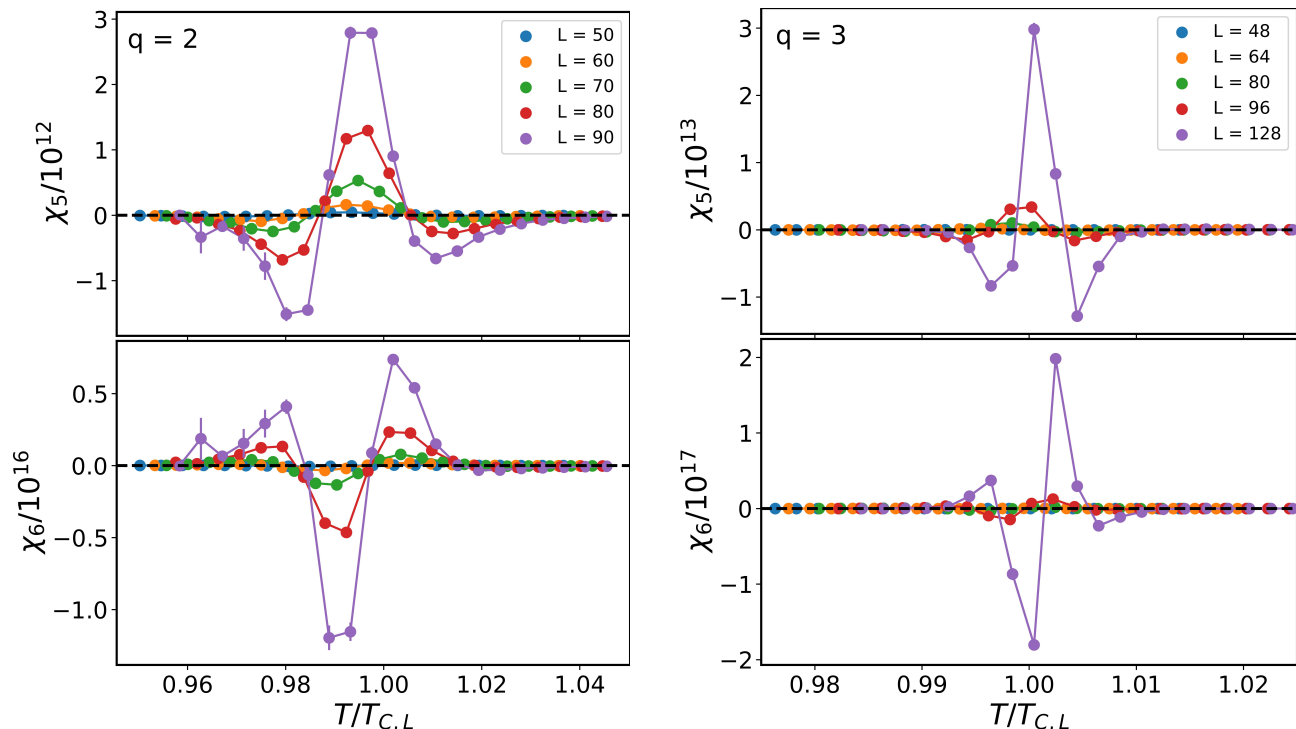


FIG. 4. The fifth and sixth order susceptibilities of magnetization, χ_5 and χ_6 , are shown for different lattice sizes as a function of temperature scaled by critical temperature of the corresponding lattice, $T/T_{C,L}$. The left side plot belongs to two-dimensional $q = 2$ state Potts model whereas the right side plot is for $q = 3$ state Potts model. The upper panel represents χ_5 and the bottom panel represents χ_6 [where χ_5 and χ_6 divided by a factor 10^{12} (10^{13}) and 10^{16} (10^{17}) respectively for $q = 2$ ($q = 3$)].

the fit are referred as e''_n . For $q = 2$ state Potts model, the values of scaling exponents are given in Table III, whereas for $q = 3$ state Potts model, they are provided in Table IV. Additionally, we compare the scaling exponents (Eq. 14) obtained using exact values of γ and ν as well as by using the estimates of γ and ν (from scaling of χ_2) obtained in this paper, and they are referred as e_n and e'_n respectively in Tables III and IV. The numerically estimated scaling exponents, e''_n for the higher-order susceptibilities show a good agreement with the analytically obtained values. We also note that determining the exponents from finite size scaling of χ_n 's instead of using the numerical estimate of γ and ν from χ_2 result in smaller numerical errors.

Quantity	e_n	e'_n	e''_n
χ_3	3.625	3.566 ± 0.097	3.608 ± 0.026
χ_4	5.500	5.420 ± 0.130	5.500 ± 0.074
χ_5	7.375	7.280 ± 0.160	7.257 ± 0.067
χ_6	9.250	9.130 ± 0.190	9.196 ± 0.066

TABLE III. Finite size scaling exponents of higher-order susceptibilities, e''_n obtained from fits to peak (or dip) values of χ_n as a function of lattice size in two-dimensional $q = 2$ state Potts model. Here, e_n is computed based on exact values of γ and ν ($\gamma = 7/4$ and $\nu = 1$) in Eq. 14, while e'_n is derived using our estimates of γ and ν discussed in Sec. IV A. The quoted values after ' \pm ' represent statistical uncertainties derived from the fit.

Quantity	e_n	e'_n	e''_n
χ_3	3.599	3.593 ± 0.036	3.619 ± 0.021
χ_4	5.466	5.458 ± 0.047	5.501 ± 0.047
χ_5	7.333	7.322 ± 0.059	7.301 ± 0.047
χ_6	9.199	9.187 ± 0.071	9.197 ± 0.077

TABLE IV. Finite size scaling exponents of higher-order susceptibilities, e''_n obtained from fits to peak (or dip) values of χ_n as a function of lattice size in two-dimensional $q = 3$ state Potts model. Here, e_n is computed based on exact values of γ and ν ($\gamma = 13/9$ and $\nu = 5/6$) in Eq. 14, while e'_n is derived using our estimates of γ and ν discussed in Sec. IV A. The quoted values after ' \pm ' represent statistical uncertainties derived from the fit.

B. Ordering of Cumulant ratios

In this section, we delve into the discussion of whether the two-dimensional $q = 2$ and $q = 3$ state Potts models exhibit ordering in the susceptibility ratios, $\frac{\chi_6}{\chi_2} < \frac{\chi_5}{\chi_1} < \frac{\chi_4}{\chi_2} < \frac{\chi_3}{\chi_1}$. Figure 5 presents a comparison of susceptibility ratios, $\frac{\chi_3}{\chi_1}$, $\frac{\chi_4}{\chi_2}$, $\frac{\chi_5}{\chi_1}$, and $\frac{\chi_6}{\chi_2}$, in the $q = 2$ state Potts model for lattice sizes of 50, 60, and 80 as a function of temperature scaled by $T_{C,L}$. The shaded yellow band corresponds to the critical region, $T_{C,L} \pm \sigma_C$, where the values of σ_C are listed in Table I. It is already clear from

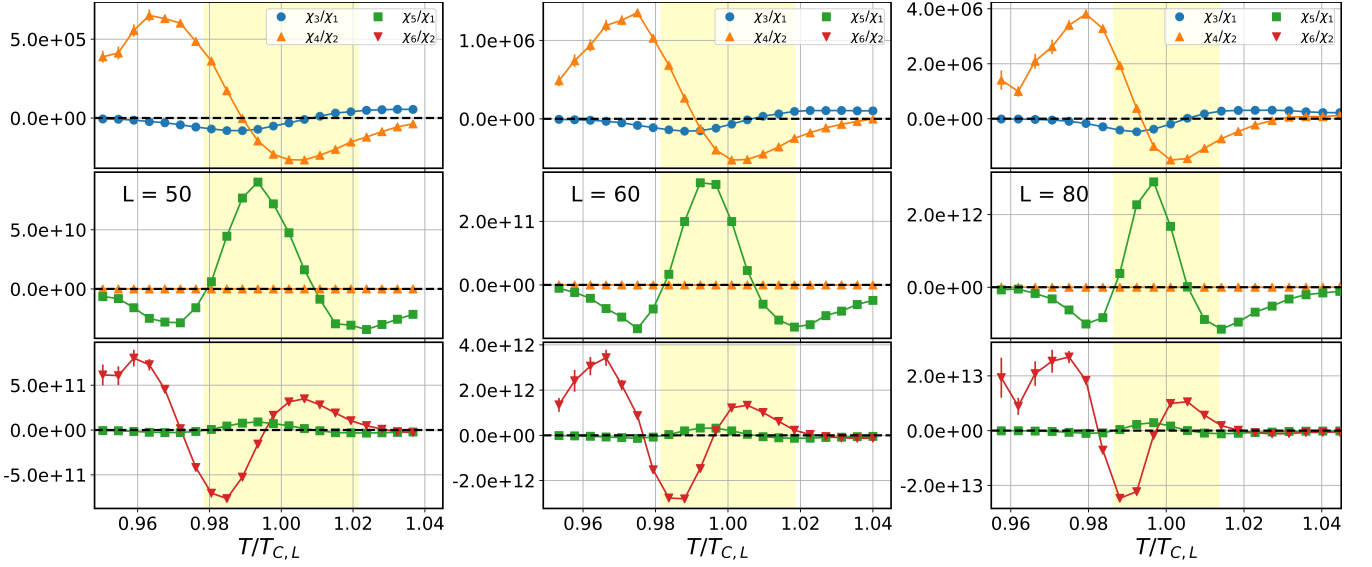


FIG. 5. Ratios of the susceptibilities, χ_3/χ_1 , χ_4/χ_2 , χ_5/χ_1 and χ_6/χ_2 for two-dimensional $q = 2$ state Potts model with lattice sizes, $L = 50$ (left plot), 60 (middle plot), and 80 (right plot) are shown as a function of scaled temperature, $T/T_{C,L}$. The yellow shaded region represents the critical region, $T_{C,L} \pm \sigma_C$.

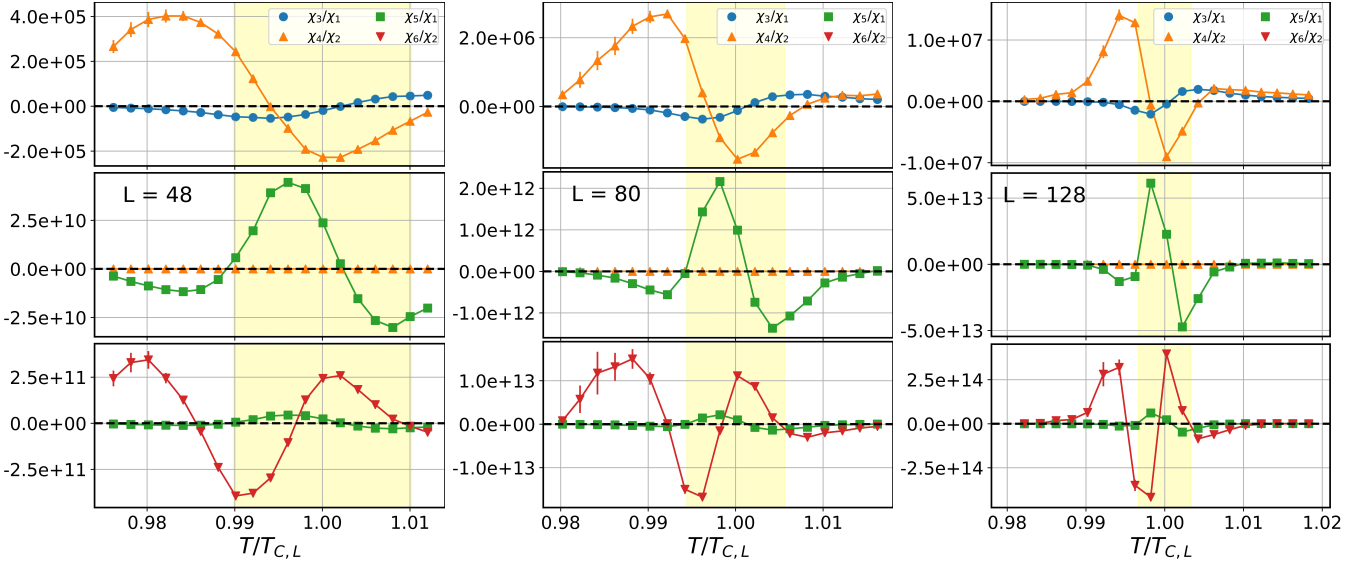


FIG. 6. Ratios of the susceptibilities, χ_3/χ_1 , χ_4/χ_2 , χ_5/χ_1 and χ_6/χ_2 for two-dimensional $q = 3$ state Potts model with lattice sizes, $L = 50$ (left plot), 60 (middle plot), and 80 (right plot) are shown as a function of scaled temperature, $T/T_{C,L}$. The yellow shaded region represents the critical region, $T_{C,L} \pm \sigma_C$.

Figs. 3 and 4 that the scale of the susceptibilities differ by factors larger than $\sim \mathcal{O}(10^3)$. Therefore, to investigate the inequalities among the susceptibility ratios (if it exists) thoroughly, the ratios are displayed pairwise in three panels (for easy inspection by eye). Furthermore, a meaningful discussion of the ordering of the ratio of susceptibilities is feasible in the critical region around $T_{C,L}$ as a result of the vast changes in the magnitudes of successively higher orders. A clear ordering, $\frac{\chi_5}{\chi_1} < \frac{\chi_4}{\chi_2} < \frac{\chi_3}{\chi_1}$ is observed for $T > T_a$ in the critical region from the top and middle panel plots of Fig. 5, where $T_a \sim 1.01T_{C,L}$

($T_a \sim 1.005T_{C,L}$) for $L = 50$ ($L = 80$). But the ordering, $\frac{\chi_6}{\chi_2} < \frac{\chi_5}{\chi_1}$ is not observed for $T > T_a$. Instead, a reverse ordering is observed, with $\frac{\chi_5}{\chi_1}$ being smaller than $\frac{\chi_6}{\chi_2}$ for the entire $T > T_{C,L}$. Therefore, we find that the expected complete ordering as seen in [11] is not observed in any temperature range near the critical region in $q = 2$ state Potts model. Only a truncated ordering of the susceptibility ratios up to $\frac{\chi_5}{\chi_1}$, i.e., $\frac{\chi_5}{\chi_1} < \frac{\chi_4}{\chi_2} < \frac{\chi_3}{\chi_1}$ holds true for $T > 1.01T_{C,L}$ across all lattice sizes shown in Fig. 5. Such a truncated inequality is not observed for the entire

temperature range, $T < T_a$.

The susceptibility ratios for the three-state Potts model are similarly examined for lattice sizes 48, 80 and 128 in Fig. 6 and similar trends are observed for the ratios as seen in the $q = 2$ state Potts model. An ordering of the ratios, $\frac{\chi_5}{\chi_1} < \frac{\chi_4}{\chi_2} < \frac{\chi_3}{\chi_1}$ is observed for $T > T_a$ within the critical region where $T_a \sim 1.002T_{C,L}$ ($T_a \sim 1.001T_{C,L}$) for $L = 48$ ($L = 80$). For the largest lattice size, $L = 128$ in Fig. 6 (right plot), the ratios show distinct differences only in a narrow region around $T/T_{C,L} = 1$ between 0.984 to 1.008, making it possible to talk of any inequality in this region around the transition point. In the top panel of the right plot, $\frac{\chi_4}{\chi_2} < \frac{\chi_3}{\chi_1}$ for $T/T_{C,L}$ in (0.996, 1.003) and the inequality is reversed for (0.984, 0.996). Similarly, in the middle panel, $\frac{\chi_5}{\chi_1} < \frac{\chi_4}{\chi_2}$ in (0.99, 0.994) and (0.999, 1.004) while inequality is reversed in (0.994, 0.999). Finally, in the bottom panel, $\frac{\chi_6}{\chi_2} < \frac{\chi_5}{\chi_1}$ in two regions of $T/T_{C,L}$, (0.993, 0.997) and (1.001, 1.006), whereas the ratio is reversed in the two complementary regions, (0.986, 0.983) and (0.997, 1.001). Therefore, it can now be easily summarized that only in a narrow range of temperature, ($1.001T_{C,L}$, $1.003T_{C,L}$), a complete ordering of ratios, i.e., $\frac{\chi_6}{\chi_2} < \frac{\chi_5}{\chi_1} < \frac{\chi_4}{\chi_2} < \frac{\chi_3}{\chi_1}$ is observed. In no other region of temperature, such an inequality or its complete reversed version is seen, including the entire region below $T_{C,L}$. As one decreases the lattice size, a similar trend is observed albeit in yet narrower interval for temperature greater than $T_{C,L}$.

A partial reversal of the ordering up to $\frac{\chi_5}{\chi_1}$, i.e., $\frac{\chi_5}{\chi_1} > \frac{\chi_4}{\chi_2} > \frac{\chi_3}{\chi_1}$ is seen in a narrow temperature range below the $T_{C,L}$, but a complete reversal is not observed for both $q = 2$ and $q = 3$ state Potts model. An important point to note is that regions of inequality exclusively lie in the critical region, which itself shrinks as in the infinite volume limit. This suggests that for infinite system size, we may not be able to establish any inequalities for the susceptibility ratios of magnetization in the spin models considered, and any observed orderings are a finite size effect. It would be interesting to check if any such volume dependence of the produced medium is seen in the relativistic heavy ion collisions.

V. CONCLUSIONS

LQCD predicts a specific hierarchy of net-baryon number susceptibility ratios near the quark-hadron transition temperature for small μ_B : $\frac{\chi_6}{\chi_2} < \frac{\chi_5}{\chi_1} < \frac{\chi_4}{\chi_2} < \frac{\chi_3}{\chi_1}$. The STAR experiment tested these predictions for net-proton number cumulant ratios in Au+Au collisions at various center-of-mass energies. Cumulant ratios from 7.7 to 200 GeV exhibited the predicted hierarchy, while a reverse ordering was observed at 3 GeV. If these inequalities are universally applicable for any system undergoing phase transition, is what we tried to understand.

In this study, we investigated higher-order susceptibilities of magnetization and their ratios in the critical re-

gions of two-dimensional two and three-state Potts models. Utilizing the Wolff cluster algorithm to mitigate critical slowing down effects, simulations were conducted. We employed finite size scaling techniques to extract scaling exponents associated with higher-order susceptibilities, extending up to the sixth order. Additionally, we estimated these scaling exponents using the known critical exponents of the model, specifically the ν and γ exponents. The obtained values from both methods exhibited a good agreement, indicating that the behavior of higher-order susceptibilities aligns well with our understanding of second-order phase transitions in the spin models.

We observed an absence of a consistent order in susceptibility ratios both above and below the pseudo-critical point (pseudo-critical temperature). A truncated ordering, $\frac{\chi_5}{\chi_1} < \frac{\chi_4}{\chi_2} < \frac{\chi_3}{\chi_1}$ is observed in a small temperature range, greater than the pseudo-critical temperature for a given lattice size in both two and three-state Potts models. In a yet narrow temperature range just above the pseudo-critical temperature, the complete ordering hierarchy in the susceptibility ratios is noted in the three-state Potts models for $L = 128$ (illustrated in Fig. 6). While a complete reversal of this ordering is not observed in either of the models, we acknowledge that a partial reversal of the ordering, $\frac{\chi_5}{\chi_1} > \frac{\chi_4}{\chi_2} > \frac{\chi_3}{\chi_1}$ is seen in a small temperature range below the pseudo-critical temperature. Furthermore, we found that the region suitable for making comparisons between these ratios diminishes notably as the lattice size (or ‘‘lattice volume’’) increases, shrinking to a point in the infinite volume limit. Consequently, the orderings observed in the susceptibility ratios can be attributed to finite size effects in spin model.

The spin models considered here have only a second order phase transition. A more realistic simulation which will be in better analogy with the expectations for the QCD phase diagram entails employing $q = 3$ state Potts model on a three-dimensional lattice and with a small but non-vanishing magnetic field. It will be interesting to see what changes does a first order phase transition or the cross over region beyond the critical magnetic field make to the above observations on the inequality structure.

ACKNOWLEDGMENTS

We acknowledge the support of the Department of Atomic Energy (DAE) and the Department of Science and Technology (DST), Government of India. RVG expresses gratitude for the financial support from DAE through the Raja Ramanna Fellowship and the hospitality of the Department of Physics at IISER Bhopal. BM and SS acknowledge the financial support of DAE and DST. We also acknowledge the use of Garuda HPC facility at the School of Physical Sciences, NISER. SS would like to thank V K S Kashyap for technical help in running simulations, as well as Ashish Pandav and Debashish Mallick for insightful discussions regarding STAR results.

- [1] Edward V. Shuryak. Quantum Chromodynamics and the Theory of Superdense Matter. *Phys. Rept.*, 61:71–158, 1980.
- [2] Heng-Tong Ding, Frithjof Karsch, and Swagato Mukherjee. Thermodynamics of strong-interaction matter from Lattice QCD. *Int. J. Mod. Phys. E*, 24(10):1530007, 2015.
- [3] Szabolcs Borsanyi, Zoltan Fodor, Christian Hoelbling, Sandor D. Katz, Stefan Krieg, and Kalman K. Szabo. Full result for the QCD equation of state with 2+1 flavors. *Phys. Lett. B*, 730:99–104, 2014.
- [4] Anton Andronic, Peter Braun-Munzinger, Krzysztof Redlich, and Johanna Stachel. Decoding the phase structure of QCD via particle production at high energy. *Nature*, 561(7723):321–330, 2018.
- [5] Y. Aoki, G. Endrodi, Z. Fodor, S. D. Katz, and K. K. Szabo. The Order of the quantum chromodynamics transition predicted by the standard model of particle physics. *Nature*, 443:675–678, 2006.
- [6] Juergen Berges and Krishna Rajagopal. Color superconductivity and chiral symmetry restoration at nonzero baryon density and temperature. *Nucl. Phys. B*, 538:215–232, 1999.
- [7] M. A. Halasz, A. D. Jackson, R. E. Shrock, M. A. Stephanov, and J. J. M. Verbaarschot. Phase diagram of qcd. *Phys. Rev. D*, 58:096007, Sep 1998.
- [8] M. Asakawa and K. Yazaki. Chiral Restoration at Finite Density and Temperature. *Nucl. Phys. A*, 504:668–684, 1989.
- [9] A. Pandav, D. Mallick, and B. Mohanty. Search for the QCD critical point in high energy nuclear collisions. *Prog. Part. Nucl. Phys.*, 125:103960, 2022.
- [10] Adam Bzdak, Shinichi Esumi, Volker Koch, Jinfeng Liao, Mikhail Stephanov, and Nu Xu. Mapping the Phases of Quantum Chromodynamics with Beam Energy Scan. *Phys. Rept.*, 853:1–87, 2020.
- [11] Bassam Aboona et al. Beam Energy Dependence of Fifth and Sixth-Order Net-proton Number Fluctuations in Au+Au Collisions at RHIC. *Phys. Rev. Lett.*, 130(8):082301, 2023.
- [12] A. Bazavov, D. Bollweg, H.-T. Ding, P. Enns, J. Goswami, P. Hegde, O. Kaczmarek, F. Karsch, R. Larsen, Swagato Mukherjee, H. Ohno, P. Petreczky, C. Schmidt, S. Sharma, and P. Steinbrecher. Skewness, kurtosis, and the fifth and sixth order cumulants of net baryon-number distributions from lattice qcd confront high-statistics star data. *Phys. Rev. D*, 101:074502, Apr 2020.
- [13] A. Bazavov, H.-T. Ding, P. Hegde, O. Kaczmarek, F. Karsch, E. Laermann, Swagato Mukherjee, H. Ohno, P. Petreczky, E. Rinaldi, H. Sandmeyer, C. Schmidt, Chris Schroeder, S. Sharma, W. Soeldner, R. A. Soltz, P. Steinbrecher, and P. M. Vranas. Skewness and kurtosis of net baryon-number distributions at small values of the baryon chemical potential. *Phys. Rev. D*, 96:074510, Oct 2017.
- [14] Wei-jie Fu, Xiaofeng Luo, Jan M. Pawłowski, Fabian Rennecke, Rui Wen, and Shi Yin. Hyper-order baryon number fluctuations at finite temperature and density. *Phys. Rev. D*, 104:094047, Nov 2021.
- [15] Szabolcs Borsanyi, Zoltan Fodor, Jana N. Guenther, Sandor K. Katz, Kalman K. Szabo, Attila Pasztor, Israel Portillo, and Claudia Ratti. Higher order fluctuations and correlations of conserved charges from lattice QCD. *JHEP*, 10:205, 2018.
- [16] Benjamin Svetitsky and Laurence G. Yaffe. Critical Behavior at Finite Temperature Confinement Transitions. *Nucl. Phys. B*, 210:423–447, 1982.
- [17] R. V. Gavai, F. Karsch, and B. Petersson. A Study of the Correlation Length Near a First Order Phase Transition: The 3-D Three State Potts Model. *Nucl. Phys. B*, 322:738–758, 1989.
- [18] L. G. Yaffe and B. Svetitsky. First-order phase transition in the su(3) gauge theory at finite temperature. *Phys. Rev. D*, 26:963–965, Aug 1982.
- [19] F Green and Frithjof Karsch. Mean field analysis of su (n) deconfining transitions in the presence of dynamical quarks. *Nuclear Physics B*, 238(2):297–306, 1984.
- [20] H. W. J. Blöte and R. H. Swendsen. First-order phase transitions and the three-state potts model. *Phys. Rev. Lett.*, 43:799–802, Sep 1979.
- [21] Frithjof Karsch and Sven Stickan. The Three-dimensional, three state Potts model in an external field. *Phys. Lett. B*, 488:319–325, 2000.
- [22] F. Y. Wu. The Potts model. *Reviews of Modern Physics*, 54(1):235–268, January 1982.
- [23] Lars Onsager. Crystal statistics. i. a two-dimensional model with an order-disorder transition. *Phys. Rev.*, 65:117–149, Feb 1944.
- [24] R. K. Pathria and Paul D. Beale. *Statistical Mechanics*. Elsevier, 3rd edition, 2011.
- [25] R. G. M. Rodrigues, B. V. Costa, and L. A. S. Mól. Moment-generating function zeros in the study of phase transitions. *Phys. Rev. E*, 104:064103, Dec 2021.
- [26] Peter J Smith. A recursive formulation of the old problem of obtaining moments from cumulants and vice versa. *The American Statistician*, 49(2):217–218, 1995.
- [27] V. Privman and M. E. Fisher. Universal critical amplitudes in finite-size scaling. *Phys. Rev. B*, 30:322–327, Jul 1984.
- [28] R.K. Pathria and Paul D. Beale. 14 - phase transitions: The renormalization group approach. In R.K. Pathria and Paul D. Beale, editors, *Statistical Mechanics (Third Edition)*, pages 539–581. Academic Press, Boston, third edition edition, 2011.
- [29] Andrea Pelissetto and Ettore Vicari. Critical phenomena and renormalization group theory. *Phys. Rept.*, 368:549–727, 2002.
- [30] Ulli Wolff. Collective monte carlo updating for spin systems. *Phys. Rev. Lett.*, 62:361–364, Jan 1989.
- [31] M. E. J. Newman and G. T. Barkema. *Monte Carlo methods in statistical physics*. Clarendon Press, Oxford, 1999.